Available online at www.sciencedirect.com

SciVerse ScienceDirect

Procedia - Social and Behavioral Sciences 53 (2012) 356 – 365

Procedia
Social and Behavioral Sciences

SIIV - 5th International Congress - Sustainability of Road Infrastructures

Characterization of reinforced asphalt pavement cracking behavior using flexural analysis

Elena Romeo[a,]*, Antonio Montepara[a]

[a]*University of Parma , Parco Area delle Scienze 181/A, Parma, 43124, Italy*

Abstract

This paper focuses on performance assessment and size effect evaluation on flexural fracture tests performed on two-layered reinforced asphalt specimens. A steel net and three fiber-glass grids were investigated. Three Point Bending tests were performed on 60mm tall specimens composed by both leveling (20mm) and wearing (40mm) layers. The test was performed on two differently-shaped specimens (400x100 mm beams and a 500x500 mm slabs) on both reinforced and not reinforced samples. Strain localization and damage distribution were investigated using an in-house Digital Image Correlation (DIC) System capable of achieving highly accurate 2D full-field strain maps of the specimens during loading.

Keywords: Reinforced Asphalt Pavement; Steel Reinforcement; Fiber-glass Reinforcement; Digital Image Correlation (DIC)

1. Introduction

One of the most common technique used to rehabilitate severely cracked pavements consists in placing an HMA overlay on the existing pavement. Rarely this approach is a long-term efficient solution since deficiencies in the old pavement are very rapidly reflected at the surface as a result of the combined effects of thermally induced stresses and traffic loading. In recent years, interlayer systems have received considerable attention as viable solutions to the problem of improving flexible pavement resistance to reflection cracking in asphalt overlays, as well as to extend the pavement's fatigue life [1,2,3]. The interlayer system is laid down either between an overlay and an existing pavement or within the pavement system. Previous researches and field analyses have shown that different types of interlayer systems (i.e. steel mesh, polypropylene and glass fiber grid, geotextile) have the capability of improving both fatigue and cracking resistance of asphalt pavement [1,4,5]. However, some of the interlayer systems used in the past have shown minimal benefits due to the lack of understanding of their mechanism [6,7]

The study presented in this paper focuses on performance assessment and size effect evaluation on flexural fracture tests performed on reinforced specimens. Four different interlayer systems were investigated: three

 doi:10.1016/j.sbspro.2012.09.887

fiberglass-grids and one double-twist steel net. The first technique consists in installing a fiberglass grid in between the leveling layer, placed on the base course to seal and level the preexisting distresses, and the wearing course (3/4 cm in depth); the second technique consists in installing a double-twist steel net at an interface between the base layer and the linking courses (60-80 mm in depth).

In order to better understand the mechanical behavior of the interlayer systems and evaluate the effects of the specimen size on the reliability of the results, the Three Point Bending (3PB) test was performed using two different specimen geometries: 500x500 mm slabs and 400x100 mm beams. The tests were performed at 20°C on reinforced and not reinforced 60 mm tall specimens to simulate a real overlay structure. Three different fiberglass reinforcements and one double-twist steel net were employed in this study. Strain localization and damage distribution were investigated using a Digital Image Correlation System (DIC) developed at the University of Parma [8,9]. The in-house developed DIC-based system, specifically studied for imaging asphalt specimen, was employed to obtain 2D full-field strain maps of specimens during tensile loading.

2. Materials and Methodologies

2.1. Asphalt Mixtures

Two different fine-graded HMA Superpave mixtures, composed by the same asphalt binder but different aggregate gradations, were used in this study. The first one is a 4.5-mm nominal maximum size mix typically used for leveling courses, while the second one is a 12.5-mm nominal maximum size mix typically used for wearing courses. Both the leveling and the wearing mixtures were designed according to the Superpave mix design procedure, resulting in 6.1% and 5.7% design asphalt content, respectively (medium traffic level).

The same natural PG 64-28 asphalt binder (NV) was used for both the mixtures. The two mixtures were tested at 10°C to evaluate their visco-elastic properties using the HMA Fracture Mechanics model developed by Roque et al. [10]. A summary of the mixtures properties is listed in Table 1.

Table 1: Properties of the two mixtures

Mixture	Resilient Modulus (GPa)	Creep Compliance @ 1000 sec (1/GPa)	Tensile Strength (MPa)	Fracture Energy (kJ/m3)
Leveling	13.84	3.46	3.71	2.06
Wearing	19.23	4.38	3.22	1.99

2.2. Reinforcements

Four different reinforcements were used in this study: three fiberglass-grids (FGA, FGB and FGC) and one double-twist steel net. The fiberglass grid configuration features fiberglass strands coated with an elastomeric polymer. Grids FGA and FGB are open fiberglass geogrids coated with an elastomeric polymer and self-adhesive glue. They differ for the mesh dimension resulting 12.5x12.5 mm for the FGA and 25x25 mm for the FGB. Grid FGC consists of 25x25 mm fiberglass strands coated with a polymer resin adhered with a thin thermoplastic film which acts as a tack coat. The steel reinforcement consists in a double-twist 8x10cm hexagonal mesh, transversally reinforced with steel wires at regular intervals of 16cm. Technical specifications are listed Table 2.

Table 2. Technical Specification of the different reinforcements

Reinforcement	Fiberglass Grid A	Fiberglass Grid B	Fiberglass Grid C	Steel Net
Tensile Strength (kN/m)	115x115	115x115	115x115	39x50
Tensile Elongation	2.5%	2.5%	2.5%	>10%
Grid Size (mm)	12.5x12.5	25x25	25x25	80x100

2.3. Specimen Preparation

Four slabs were prepared for each interlayer system. Aggregate batches were prepared to produce 500x500x60mm slabs. The aggregates, the asphalt binder and mixing equipment were heated for three hours at 160°C to achieve appropriate uniform mixing temperature. The batches were then mixed with the design asphalt content percentage and heated for another two hours at 135°C for short-term aging.

The slabs were compacted on a proper compactor set to produce 500mm long by 500mm wide specimens. This equipment is made up of a cylindrical horizontally pivoted steel cup upon which a 3ton maximum load hydraulic press is placed. Below the press, a 500x500mm mobile basement is placed with the formwork containing the material. This formwork moves while the pivoted element applies a given pressure to compact the material to the desired air void percentage, in this case 6 (±0.5) per cent.

Fiberglass grid reinforced specimens were prepared compacting each layer separately starting from the leveling layer (20mm) and then adding the wearing course (40mm). The grid was inserted immediately after the leveling layer compaction. For assuring a good adhesion, the grid was also rolled on the leveling layer applying a lower pressure. FGA and FGB reinforcements were also coated using a thin film of natural asphalt binder (NV). Steel net reinforced specimens were prepared laying the reinforcement at the base of the specimen, then compacting the wearing course (40 mm) and finally pouring and compacting the surface layer composed by the leveling mixture (20 mm). For each interlayer system, one slab was sawn to obtain four effective beams, each 10 mm thick discarding the lateral parts for reducing density gradient effects.

3. Three Point Bending Test

The Three Point Bending (3PB) test was employed using two differently-shaped specimens: a 400x100 mm beam specimen and a 500x500 mm slab specimen. The tests were performed on three replicates at 20°C using an MTS closed-loop servo-hydraulic loading system on both reinforced and unreinforced specimens. The static load transmission occurs in the middle section of the specimen with a displacement control system, where the top loading ring drops at 0.084mm/s. The span length of the specimen is settled at 0.8 the beam length. The digital camera was located inside the climatic chamber to acquire an image sequence of the specimen during loading at 10 frame per second, grabbing a 80x60 mm area at the center of the specimen. The three point bending test experimental set up is shown in Figure 1.

Strain localization and crack patterns were monitored using a Digital Image Correlation System (DIC) capable of obtaining highly accurate 2D full-field strain maps of specimens during loading. The technique utilizes a matching algorithm that automatically establishes correspondences between grey value windows extracted from digital images. The sequence of images is acquired with a digital camera Basler piA1600-35gm (resolution 1608x1308, focal length 8mm, pixel size 7.4 micrometers, 35 fps@max resolution) during testing. The image

matching technique is applied to track a set of features artificially generated on the specimen surface. More details are described by Birgisson et al. [8].

beam specimen slab specimen

Fig. 1. Three Point Bending Test experimental

4. Experimental Results

4.1. Three Point bending Test on Beams

Three replicates were performed for each type of reinforcement as well as for the not reinforced specimen, monitoring strains with DIC analyses. Figure 2 shows force-deflection (a) and stress-strain (b) curves obtained from the four reinforced and the not reinforced specimens. The results highlight the important contribution provided by the reinforcements. The peak load reached by reinforced specimens is significantly higher than the maximum load reached by the not reinforced one, with factors of enhancement in effectiveness of about 1.5 (Table 3). However, the scatter among the peak loads reached by the reinforced specimens is very poor.

The different contribution provided by the reinforcements can be noted in the post-peak behavior. Fiberglass C differs much from the others, showing a second hardening phase after softening (post-first force dropping). This post-peak response assures the preservation of an asymptotical residual resistance. Fiberglass grid A and the steel net determine a less abrupt softening than Fiberglass grid B, maintaining a higher residual resistance over time. Also, reinforced specimens exhibit a better response in terms of energy dissipation. The resistance contribution provided by the reinforcements is quantifiable in terms of Fracture Energy, considering the area under the load-displacement curve that exceeds the not reinforced one [11]. As shown in Table 3, Fiberglass grid C Fracture Energy is twice than the other reinforcements. Tensile stress-strain responses confirm what observed from load-displacement results. Similar stresses at fracture were obtained for all the reinforcements. Conversely, the fracture energy density, defined as the energy required to crack the pavement structure [12] is strongly enhanced by the presence of Fiberglass grid C. In detail, Fiberglass C allows the pavement structure to deform much more before the damage becomes great enough for initiating a crack, resulting in a failure strain 4 times higher than the other reinforced specimens (Table 4).

During testing, horizontal strains at the central bottom edge of the beam specimens were monitored: a 6x6 cm area surrounding the central portion of the beam was imaged and processed to obtain full-field tensile strain maps. Figure 3 shows full-field tensile strain maps for the five pavement systems. The maps were selected at fracture point and after failure (post-peak). The difference between reinforced and not reinforced specimens is well evident. Strain maps obtained from fiberglass-reinforced specimens show highly concentrated strains localized in the bottom layer (linking layer), meaning that the reinforcement acts as a barrier to reflection cracking avoiding the propagation of cracks to the surface layer (i.e. new overlay). Steel-reinforced specimen

shows strains largely distributed through a wide area, developing in multiple locations around the fracture point. This can be attributable to the development of large tensile stresses at the bottom edge of the specimen and significantly predominant compressive stresses in the upper layer. Conversely, the strain maps obtained from the not reinforced specimen show a big crack developing in the central region which extends from the bottom edge to the surface layer along the vertical plane. Tensile strain maps also highlight the effect of reinforcement on damage distribution. Reinforced specimens maps show highly concentrated strains developing in small areas corresponding to the location of impending fracture, while the not reinforced specimen exhibits significant damage developing in a fairly big area along the vertical plane.

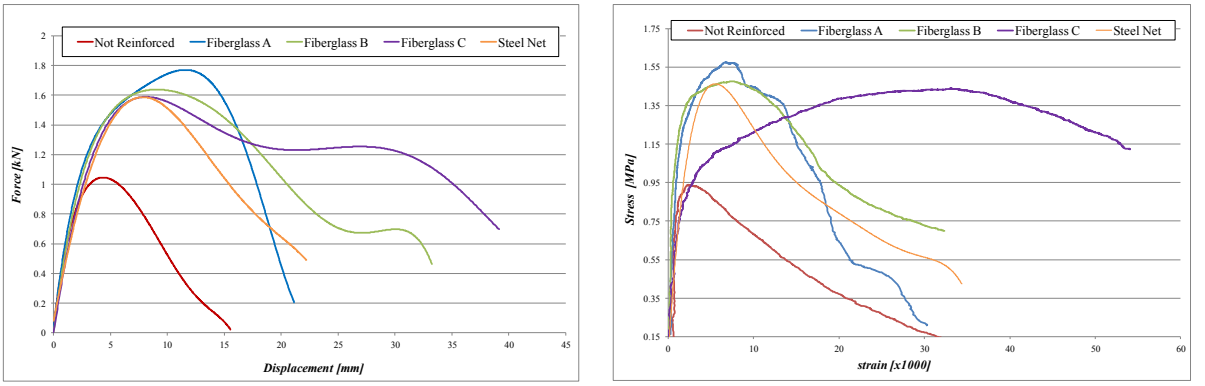

Fig. 2. (a) Load-Displacement and (b) Stress-Strain curves obtained from beams

Table 3. Peak Loads and Fracture Energies of the different interlayer systems

Reinforcement	Not Reinforced	Fiberglass Grid A	Fiberglass Grid B	Fiberglass Grid C	Steel Net
Peak Load (kN)	1.08	1.80	1.67	1.64	1.60
Fracture Energy (kJ/m2)	1.32	4.56	3.77	8.27	3.73

Table 4. Critical Parameters of the different interlayer systems

Reinforcement	Not Reinforced	Fiberglass Grid A	Fiberglass Grid B	Fiberglass Grid C	Steel Net
Critical Stress (MPa)	0.96	1.60	1.49	1.46	1.42
Critical Strain (x1000)	1.99	7.59	7.54	28.74	7.26
Fracture Energy Density (kJ/m^3)	1.23	10.18	10.07	33.84	8.8

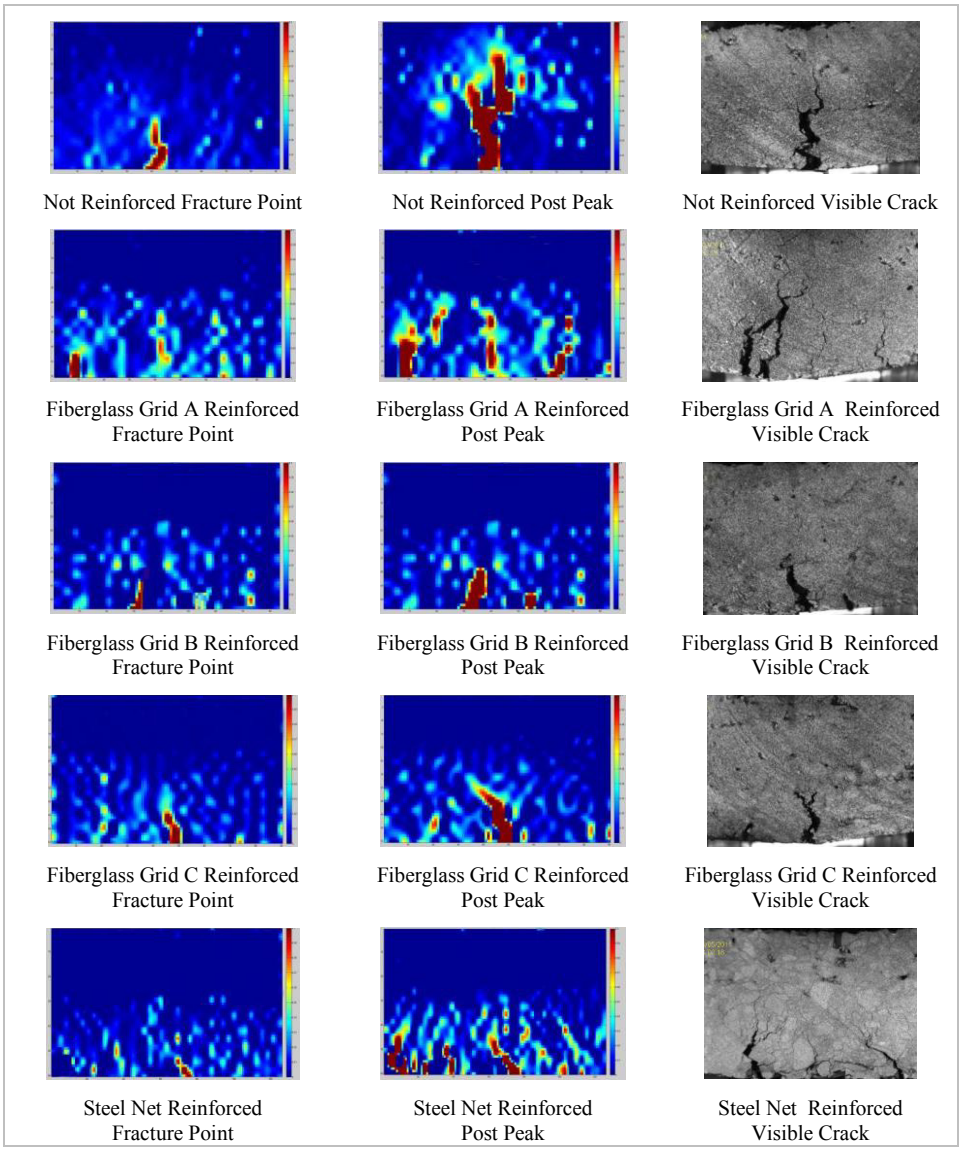

Fig. 3. Strain maps obtained from beams

4.2. Three Point Bending Test on Slabs

Force-deflection curves obtained from slab bending tests are shown in Figure 4. It's clearly evident that the presence of the reinforcement is able to enhance the ductile properties of the pavement structure. The load-displacement behavior results qualitatively similar up to fracture initiation. Then the different contributions given

by the reinforcements become significant. The not reinforced specimen exhibits a mechanical behavior typical for flexible pavements: the elastic response is maintained up to fracture initiation followed by a small yield phase until ultimate load is reached. A similar response is obtained from fiberglass A-reinforced specimen, with an increase of more than 50% in the maximum load. The load-displacement response of fiberglass B-reinforced specimen starts to deviate when fracture reaches the interface: the presence of the reinforcement makes the system more ductile deferring the ultimate failure. Fiberglass C and steel net reinforcements allow the specimens to deform more plastically before failure meaning that higher strain levels (three times more than the other two reinforcements) are required to damage the pavement structure.

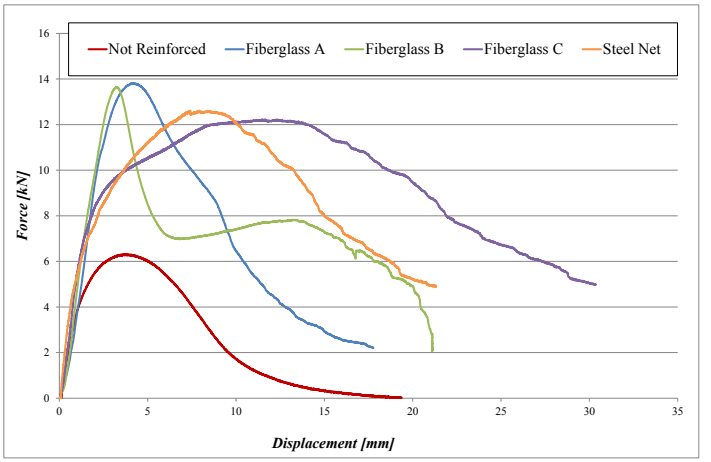

Fig. 4. Load-displacement curves obtained from slabs

In terms of fracture energy, defined as the energy required to deflect the specimen, the presence of the reinforcement is able to increase the pavement cracking resistance from 3 to 10 times (Table 5). The primary benefit of the reinforcement is to significantly reduce tensile stresses in the surface layer, shifting the maximum tensile and shear stress from the bottom of the surface layer to the bottom of the interlayer itself, thus reducing the fracture potential in the surface. This implies that the reinforcement is effective before the crack has reached it. Fiberglass C and steel reinforcements performed best, with factor of enhancement in performance of about 10 and 7 over the not reinforced specimen, respectively. This is attributable to the high bond strength developing between the reinforcements and the surrounding asphalt mixture. The good adhesion is given by different mechanical interactions depending on the type of reinforcement. Fiberglass grid C is coated with a thin thermoplastic film which acts as a tack coat and guarantees a strong bond between the asphalt layers. Steel reinforcement has a three dimensional structure, allowing the asphalt matrix to envelop each wire strand and ensuring good interlock with the aggregate skeleton.

Table 5. Critical parameters obtained from slabs

Reinforcement	Not Reinforced	Fiberglass Grid A	Fiberglass Grid B	Fiberglass Grid C	Steel Net
Peak Load (kN)	6.30	13.82	13.63	12.23	12.61
Fracture Energy (kJ/m^2)	6.19	22.70	19.66	52.86	47.57

Full-field strain maps were also obtained for slabs using the same procedure used for beams. Figure 5 shows full-field tensile strain maps obtained for not-reinforced and reinforced slab specimens. As previously observed, fiberglass-reinforced specimens show highly concentrated strains localized in the bottom layer.

The same behavior can be observed for steel-reinforced slabs. Not-reinforced specimen exhibits crack propagation up to the surface layer. Moreover, the strain distribution is totally non homogeneous showing different localization areas from which many cracks occur (at 30% of the ultimate load) and later propagate randomly. Conversely, reinforced specimens show a more localized damage distribution: crack initiation occurs in a well-defined area at 40-50% of the ultimate load.

4.3. Specimen size dependency

Tensile strength and Fracture Energy in heterogeneous materials have for long time been known to depend on the specimen size [13, 14, 15].

At low load levels, stiffness and tensile response appears to be relatively similar since localized damage does not occur. The flexural response is strongly influenced by the specimen size after ultimate load is reached or rather after damage localization. Table 6 compares ultimate loads and fracture energies obtained from beams and slabs. The ratio of slab-beam peak loads does not vary significantly. Slab ultimate load is always from 6 to 8 times the ultimate load of the respective beam configuration.

Different results are observed in terms of fracture energies. Slab-beam ratios are very similar for not-reinforced and fiberglass-reinforced specimens but vary considerably for the steel-reinforced one. In the first phase, in which the elastic response is predominant, the two curves are comparable.

Significant differences start from crack initiation up to the maximum load and in the post-peak behavior. The beam configuration does not allow for capturing the tensile stress support provided by the steel reinforcement. The beam geometry (400x100 mm) results not adequate for investigating the bi-directional contribution of the interlayer system, since steel reinforcement consists in a double-twist 8x10cm hexagonal mesh, transversally reinforced with steel wires at regular intervals of 16cm. Using a 500x500 mm specimen, the reinforcement acts in both x and y directions optimizing load transfer and shear resistance and providing better aggregate interlocking.

Thus, the slab configuration describe more realistically the mechanical behavior of the steel-reinforced interlayer system.

Table 6. parameters obtained from slabs

Reinforcement	Not Reinforced	Fiberglass Grid A	Fiberglass Grid B	Fiberglass Grid C	Steel Net
BEAM Peak Load (kN)	6.30	13.82	13.63	12.23	12.61
SLAB Peak Load (kN)	1.08	1.80	1.67	1.64	1.60
RATIO Slab/Beam	5.83	7.68	8.15	7.45	7.88
BEAM Fracture Energy (kJ/m^2)	6.19	22.70	19.66	52.86	47.57
SLAB Fracture Energy (kJ/m^2)	1.32	4.56	3.77	8.27	3.73
RATIO Slab/Beam	4.68	4.97	5.21	6.39	12.74

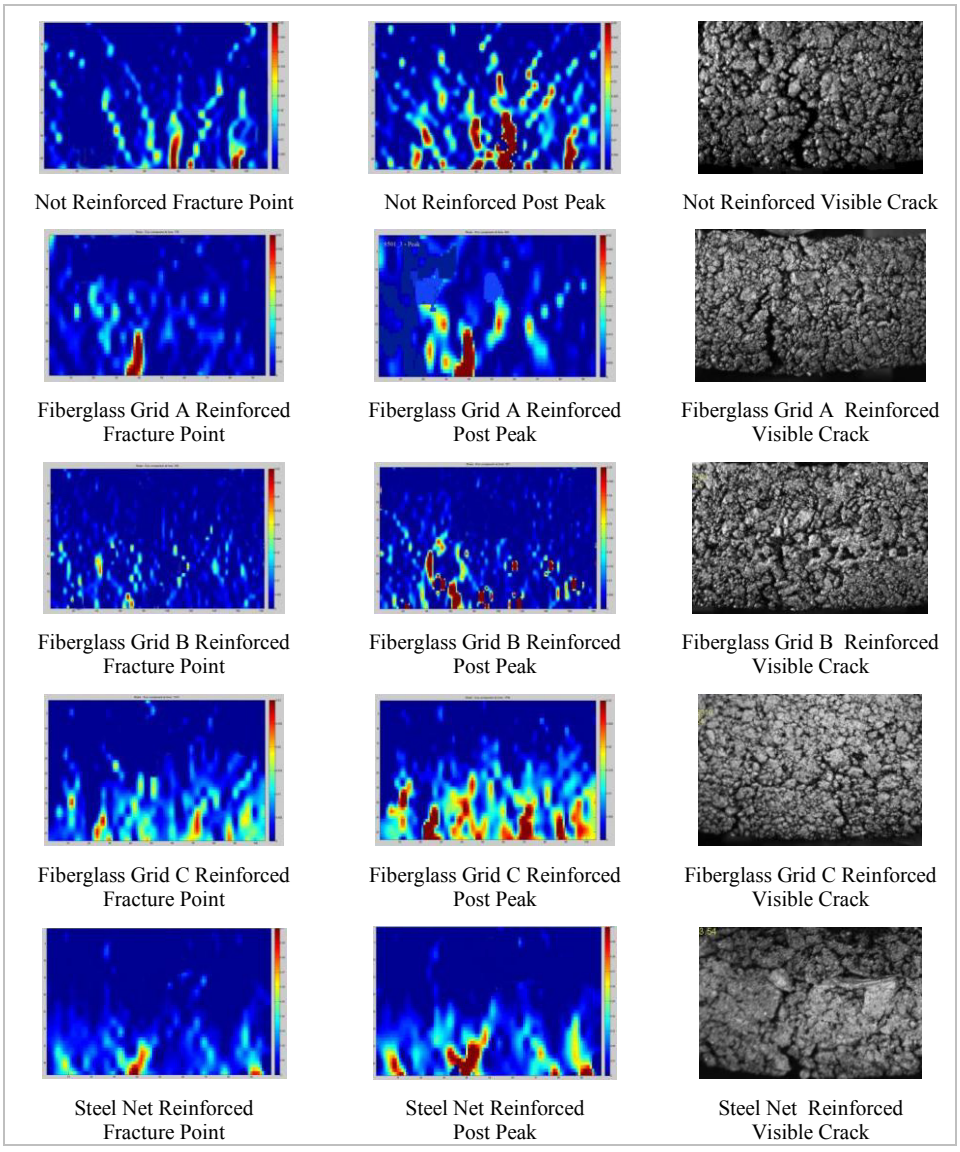

Fig. 5. Strain maps obtained from slabs

5. Conclusions

Flexural fracture tests were performed on both slabs and beams to assess the performance of reinforced pavements and to evaluate the effect of the specimen size their cracking behavior. Four different interlayer systems were investigated: three fiberglass-grids and one double-twist steel net. A Digital Image Correlation (DIC) System was employed to investigate strain localization and damage distribution in both beam and slab specimens. The results presented highlight the benefits of the reinforcements in terms of failure resistance and

energy dissipation. The different contribution given by the single reinforcement becomes evident in the post-peak behavior. Fiberglass A (12.5x12.5 mm mesh) exhibits a mechanical behavior similar to the not reinforced specimen with an increase of more than 50% in the maximum load. Fiberglass B (25x25 mm) makes the system more ductile deferring the ultimate failure. Fiberglass C (25x25 mm with thermoplastic film) and steel net reinforcements allow the specimens to deform more plastically before failure.

The primary benefit of the reinforcement is to significantly reduce tensile stresses in the surface layer shifting the maximum tensile and shear stress from the bottom of the surface layer to the bottom of the interlayer itself, thus reducing the fracture potential in the surface. Fiberglass C and steel reinforcements perform best due to the high bond strength developing between the grids and the surrounding asphalt mixture.

It was observed that specimen geometry influences only the cracking behavior of steel-reinforced system. Steel net consists in a double-twist 80x100 mm hexagonal mesh, transversally reinforced with steel wires at regular intervals of 160 mm, thus a 100 mm width specimen results not adequate for investigating the bi-directional contribution of the interlayer. Conversely, a 500x500 mm specimen allows the reinforcement to act in both x and y directions optimizing load transfer and shear resistance and providing better aggregate interlocking.

References

[1] Brown S.F., Thom N.H. & Sanders P.J. (2001). A Study of Grid Reinforced Asphalt to Combat Reflection Cracking. Journal of the Association of Paving Technologists. 70, 543-571.
[2] Al-Qadi I.L., Elseifi M. & Leonard D. (2003). Development of an Overlay Design Model for Reflective Cracking with and without Steel Reinforcing Nettings. Journal of the Association of Paving Technologists.72, 388-423.
[3] Montepara A., Tebaldi G. & Costa A. (2007). A surface steel reinforcement for pavement rehabilitation. ICPT2007 - Special ICPT Sympoisum 2007 Road Construction and Maintenance Tecnology in China. Beijing (China).
[4] Buttlar, W. G., Bozkurt D., & Dempsey B. J. (2000). Cost-Effectiveness of Paving Fabrics Used to Control Reflective Cracking. Transportation Research Record 1117, 139–149.
[5] Cleveland, G. S., Button J.W. & Lytton R. L. (2002). Geosynthetics in Flexible and Rigid Pavement Overlay Systems to Reduce Reflection . Cracking. Research Report 0-177701, Texas Transportation Institute, College Station, TX.
[6] Predoehl, N. H. (1989). Evaluation of Paving Fabric Test Installation in California Final Report. California Department of Transportation, Translab.
[7] Steinberg, M. L. (1992). Geogrid as a Rehabilitation Remedy for Asphaltic Concrete Pavements. Transportation Research Record 1369, 54–62., Washington, D.C.
[8] Birgisson B., Montepara A., Romeo E., Roque R., Roncella R., Tebaldi G. (2009). An Optical Strain Measurement System for Asphalt Mixtures. Materials and Structures. 42, 427-441.
[9] Birgisson B., Montepara A., Romeo E., Roque R., Tebaldi G. (2010). Influence of mixture properties on fracture mechanisms in asphalt mixtures. Road Materials and pavement Design, 11 (Special Issue), 61-88.
[10] Roque R., Birgisson B., Sangpetgnam B., Zhang Z. (2002). Hot Mix Asphalt Fracture Mechanics: A Fundamental Crack Growth Law for Asphalt Mixtures. Journal of the Association of Asphalt Paving Technologist, 71, 816-827.
[11] RILEM Technical Committee 50 (1985). Determination of Fracture Energy of Mortar and Concrete by means of three-point bend tests on notched beams. Materials and Structures, 18, 287-290.
[12] Zhang Z., Roque R., Birgisson B. and Sangpetgnam B. (2001). Identification and Verification of a Suitable Crack Growth Law. Journal of the Association of Asphalt Paving Technologists, 70, 206-241.
[13] Bazant, Z.P. (1993). Size effect in tensile and compressive quasibrittle failures. JCI International Workshop on Size Effect in Concrete Structures, 141–160.
[14] Carpinteri, A., Chiaia, B. & Ferro, G. (1994). Multifractral Scaling Law for the Nominal Strength Variation of Concrete Structures. Size Effect in Concrete Structures, E &FN Spon, 409–416.
[15] Shah, S.P. and McGarry F.J. (1971). Griffith fracture criterion and concrete. Journal of Engineering Mechanics, ASCE 97, 1663–1676.